DOI: 10.21062/mft.2023.021 http://www.journalmt.com

Effect of Laser Traverse Speed during Laser Hardening on Hardness Distribution and Microstructure of Hot Work Tool Steel H11

David Hradil (0000-0001-8869-6951)[1], Zbyšek Nový (0000-0001-6976-1578)[1], Josef Hodek (0000-0003-4013-9819)[1], Martina Koukolíková (0000-0002-6161-6832)[1], Adam Szyszko (0000-0002-0138-1867)[2]
[1]COMTES FHT a. s., Prumyslova 995, 334 41 Dobrany. Czech Republic. E-mail: dhradil@comtesfht.cz
[2]Warsaw University of Technology, Pl. Politechniki 1, 00-661 Warsaw, Poland.

The paper describes the effect of laser traverse speed during laser hardening on hardness and microstructure. The experimental material is hot work tool steel AISI H11 with samples sized 100×100×35 mm. The initial state of the material before laser hardening is quenched and tempered. The laser hardening temperature is constant at 1100 °C, selected laser traverse speed was 1, 2, 4, and 6 mm/s. A numerical simulation performed in DEFORM-3D software before the experiment showed tendencies of temperature displacement and expected course of hardness. Increasing traverse speed leads to decreased laser-hardened depth and decreased hardness drop in the heat-affected zone (HAZ). The experimental program confirmed the results of the numerical model. The differences in the microstructure were investigated by light (LM) and scanning electron microscopes (SEM), which revealed an evident difference between the surface area and the locality with the lowest hardness. Local differences from the perspective of presence of carbides were analysed by energy dispersive spectroscopy (EDS). This investigation was performed to optimize laser traverse speed to improve the subsurface hardness profile, which is essential for the lifetime and reliability of forging dies.

Keywords: Laser hardening, Hardness, Numerical model, Microstructure, EDS analysis

1 Introduction

Laser surface hardening (LSH) is a process in which the surface is hardened by transformation and heating of the surface is performed using laser technology. The laser beam is focused locally and traverses the surface of the material, leaving behind strips of transformed material. Due to the limited spot size of the laser beam and the relatively high thermal conductivity of steel, quenching is done not by external cooling but by the conduction of heat into the core of the processed body. By that means an extremely high cooling speed is achieved leading to a fine hardened microstructure [1–4]. Due to the nature of the interaction between electromagnetic waves (such as light) and the solid material, each laser interacts slightly differently with the surface. It has been proven that depending on the wavelength of the laser beam the absorptivity of energy will differ. In steel, the general correlation is a rise in absorption with a decrease in wavelength [5]. The laser hardening process makes it possible to make a hardened layer in different steel grades with varying results. Typically, a laser hardening depth between 0.15 and 2.3 mm is achieved. The hardness varies between 650HV and 900HV [6]. There are many parameters that change the final outcome of surface hardening. Most notable are the laser power, the traverse speed of the laser, the size and shape of the laser spot, and the beam energy profile.

One frequently reported problem is a drop in hardness in the heat affected zone. Such hardness drop was reported in research that studied steel after quenching and tempering. It was observed in steel grades AISI 434 [6], and AISI H11 [7, 8] that were bulk heat treated before laser hardening. The hardness drop results from the over-tempering effect that takes place when the area is heated above the initial tempering temperature but not austenitised (even partially). Heat is conducted into the core of the material. The second issue important to consider is the so-called back tempering effect. The back tempering effect can be described as an unwanted change in microstructure in already created hardened strips due to the creation of concurrent strips. The excessive heat that is transferred by conduction to adjacent strips can lead to a strong tempering effect. The resulting change in microstructure leads to the formation of a zone with decreased hardness. This effect was widely discussed by Giorleo et al [9]. The article showed that strength after tempering is a function of temperature, in contrast to standard bulk tempering, where the tempering effect is a function of both temperature and time. There was no correlation between the time that material was affected by temperature and strength after tempering. It is also important to note that the tempering effect only occurred when the temperature was higher than 200°C and the effect was greater at higher temperatures.

Investigation of LSH focused on AISI H11 is less

usual than the processing of slightly more alloyed AISI H13 with a higher content of vanadium [8, 10]. The laser hardening was performed after quenching and tempering. The present study deals with a different traverse speed of laser hardening. The conducted analysis was based on a preliminary numerical simulation of hardness profile behavior and subsequent detailed metallographic analysis in the LSH state with the most promising parameters of processing.

2 Material and methods

The experimental steel for these experiments was AISI H11 chromium tool steel (equivalent to DIN 1.2343) with the chemical composition shown in Tab. 1. The experimental samples were approx. 100 × 100 × 35 mm in size with a finely milled surface. These blocks were heat treated by quenching in a vacuum atmosphere at 1040 °C for 30 minutes with subsequent cooling by nitrogen pressure, followed by tempering. The tempering temperature was 575 °C with a dwell time of 2 hours. After this processing the material has a hardness of about 550-570 HV30 (corresponding to 52 – 53 HRC), and is the initial state for the laser processing.

LSH was carried out by controlling the surface temperature during the process. The temperature was kept constant at 1100 °C for all the performed processes. The experiment was based on the investigation of the variation of laser traverse speed influence on the microstructure and hardness profile of the processed samples' surface. The selected values of laser traverse speed were 1, 2, 4 and 6 mm/s. Phenomena that were investigated were surface hardness, the course of the hardness distribution, the depth of the laser-hardened area, and the drop in hardness and the microstructure in the laser hardened area.

Tab. 1 *Chemical composition of AISI H11 tool steel, wt %*

C	Si	Mn	P	S	Cr	Mo	V	Fe
0.40	1.04	0.35	0.017	0.006	5.24	1.17	0.36	Bal.

Metallographic preparation involved grinding and subsequent polishing using a standard metallographic procedure performed on Tegramin 30 equipment. The microstructure of H11 steel was revealed by Villela-Bain etchant. Metallographic observation was performed on a Nikon Eclipse MA200 light microscope (LM) equipped with NIS Elements 5.2 digital image processing and analysis software. Detailed microstructural analysis was observed on a JEOL IT 500 HR scanning electron microscope with an Octane Elite Super. The data acquisition, analyses and post-processing were performed using the software TEAM 4.5. Hardness profile HV1 was measured using a Struers DuraScan 50 laboratory hardness tester according to ISO 6507-1. The measurement was performed in the central part of the laser track from the surface with a step of 0.1 mm. Size of prior austenite grains was measured according to the ISO 643 standard test method.

The temperature distribution on the test sample for a speed of 1mm/s was recorded using welded K-type thermocouples. The distribution of thermocouples on the sample and the sample after heat treatment are shown in Fig. 1.

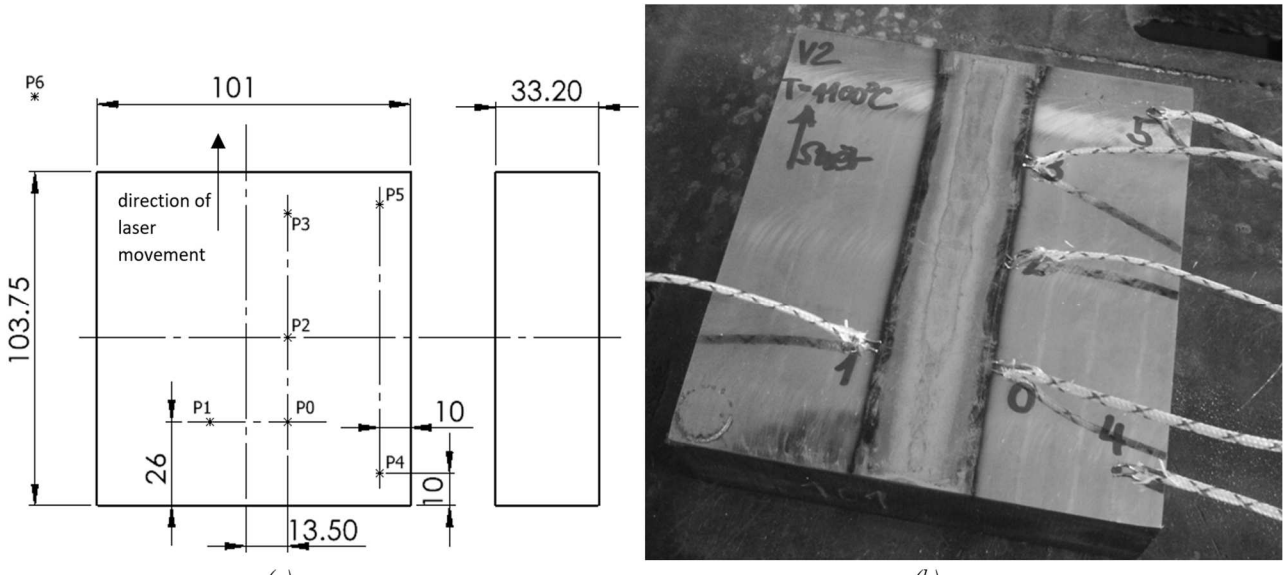

(a) *(b)*

Fig. 1 *(a) CAD and distribution of thermocouples on the sample (P6 is the ambient temperature); (b) sample after heat treatment*

3 Results

3.1 Material and numerical model

The FEM model was created in DEFORM-3D as axisymmetric - Fig. 2. Material data were generated in the software JMatPro based on the chemical composition in Tab. 1. The model was calibrated according to the measured temperatures so that the measured and calculated temperatures were in good agreement. The model contained 160800 brick elements with finer mesh in the laser heat treatment region. The heat transfer coefficient on the surface of the model was set to 5 W/m²K for an ambient temperature of 10 °C according to experience. The laser heat treatment was implemented using the heat flux boundary condition of Fig. 2 to achieve a max. temperature consistent with the experimental measurements. The measured and calculated temperatures were in good agreement. This statement is demonstrated in Fig. 2, where the measured and calculated temperatures are shown.

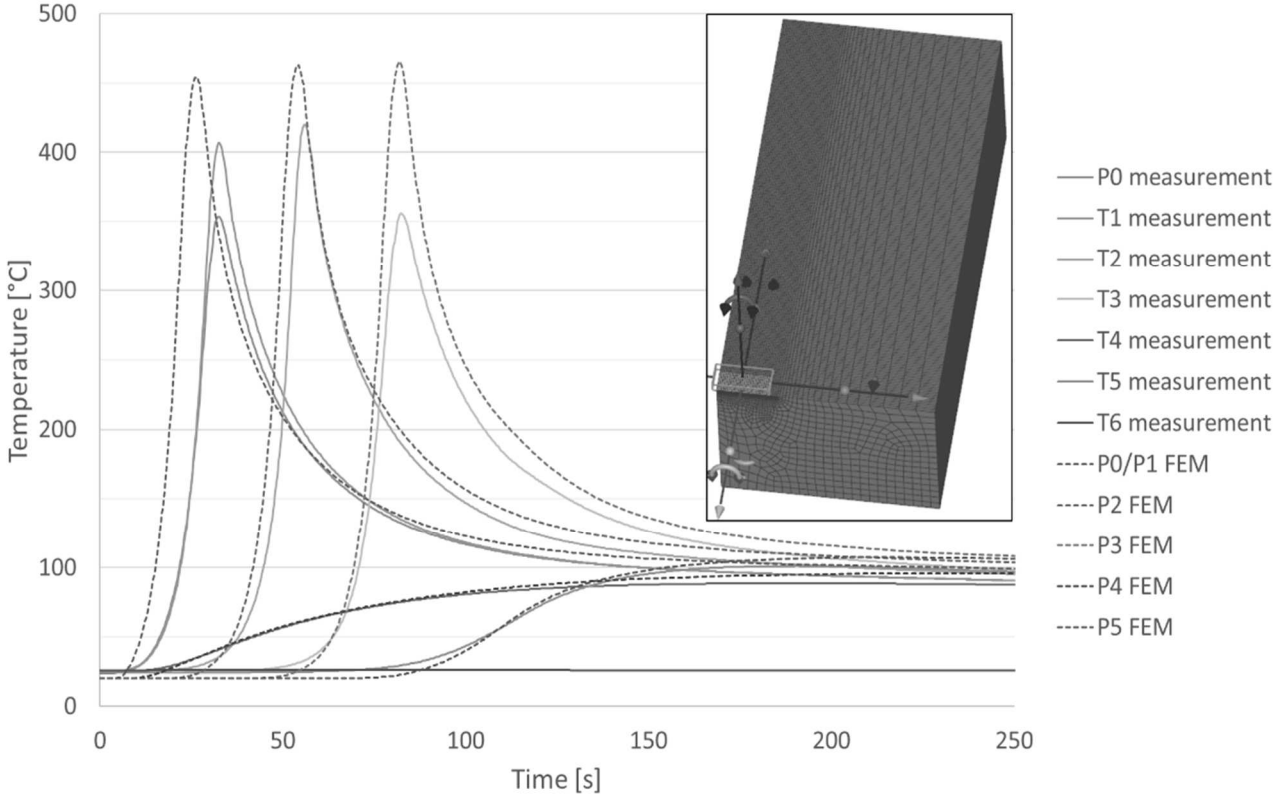

Fig. 2 *FEM model of laser heat treatment – measured and calculated temperatures at the points (as shown in* Fig. 1 *(a)) where the temperature was measured, model with the mesh and window used to describe the laser heat treatment (top right)*

Temperature-dependent changes in hardness were considered in the model through phase transformations. The initial structure (SS) - martensite transitions, changes to an intermediate structure (IS) upon heating and then to austenite (AS) upon reaching the austenitizing temperature. Upon cooling, either the intermediate structure is cooled or the austenite transforms to martensite with a different hardness (FS) than the initial structure. The kinetics of the transformations from initial structure to intermediate structure (SS-IS) and from intermediate structure to austenite (IS-AS) are described by a simplified diffusion function, based on the simplified Avrami equation (1) and it is defined by a function of the following form: this formula is an appropriate first approximation for a diffusion-based transformation. The parameters of the transformations are given in the following Tab. 2. The AS-FS transformation is described by the temperatures martensite start 339 °C and martensite 50 % 304 °C. The hardnesses of each structure are set to the following values based on measurements:

- Initial structure (SS) - 550HV
- Intermediate structure (IS) - 400HV
- Final surface martensitic structure (FS) - 730HV

$$\xi = 1 - e^{A\left(\frac{T-T_s}{T_e-T_s}\right)^D} [-] \quad (1)$$

Where:
ξ …Volume fraction transformed [-],
A, D…Chosen constants [-],
Ts…Start temperature of the transformation [°C],
Te…End temperature of the transformation [°C],
T…Average element temperature [°C].

Tab. 2 *Used parameters of the transformation*

	SS-IS	IS-AS
A	-10	-10
D	2	2
Ts	685 °C	760 °C
Te	720 °C	1050 °C

Using the model defined in this way, the variants that were heat treated were calculated. Fig. 3 shows an example of the temperature distribution in the plane of symmetry and on the surface when the laser was halfway along the path. The figure shows how the temperature spreads over the surface and inside the sample volume.

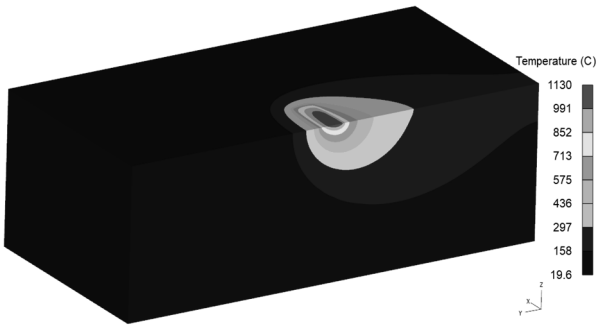

Fig. 3 *The temperature distribution in the plane of symmetry and on the surface of the sample*

The dependence of the max. temperature reached at different depths from the surface for different laser traverse speeds is shown in Fig. 4. With increasing traverse speed the depth of the heat affected zone lessens – results corresponding with the hardness profiles shown in Fig. 5. From the results we can infer that the critical temperature that leads to maximum hardness drop is about 750 °C in HAZ.

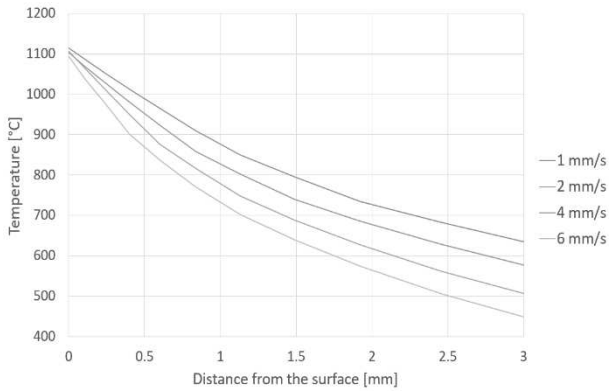

Fig. 4 *The numerical modelling of max. temperatures achieved at different depths from the surface for different laser traverse speeds*

The dependence of hardness on depth for different laser traverse speeds is shown in the following Fig. 5. Maximum depth with higher hardness compared to the initial structure is in-depth of about 1.25 mm for traverse speed 1 mm/s, then the drop of the hardness is up to depth 1.9 mm with subsequent increase of the hardness up to the initial state. With increasing traverse speed, the depth of the laser-hardened layer lessens, and the effect of the hardness drop is present at all used speeds.

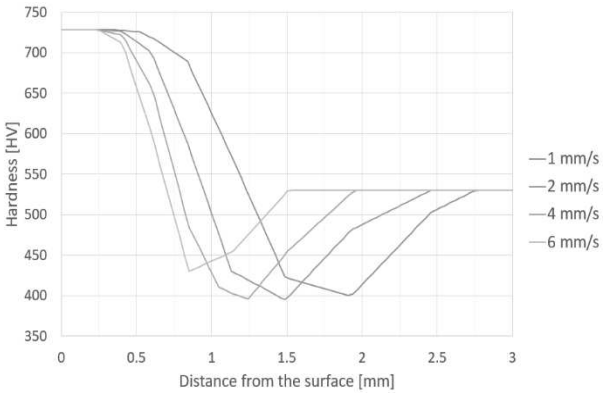

Fig. 5 *The numerically computed dependence of hardness on depth for different laser traverse speeds*

3.2 Hardness distribution

From the results shown in Fig. 6 emerge the following conclusions. At the slowest traverse speed, we obtain the highest surface hardness and the maximum depth of laser hardened layer. However, at the same time, the size of the heat-affected area increases, which causes a rapid drop in hardness beyond the laser hardening area. As the traverse speed increases, the hardness profile and laser hardening depth decrease. The core hardness is in all cases around 570-580 HV. Namely, the highest surface hardness achieved is 730-740 HV1 and was almost the same for all tested speeds. The maximum depth of laser hardening layer achieved is approx. 1.6 mm (corresponds to the depth where the hardness is higher compared to the original core hardness). The drop in hardness is similar for speeds 1 and 2 mm/s, while with increased traverse speeds of 4 and 6 mm/s the drop is not so significant, with a minimum hardness of about 460 HV1. The maximum hardness drop in the HAZ is up to 405 HV1. The hardness drop area represents the location with over-tempered martensite. For the metallographic analysis the traverse speed 1 mm/s (blue line) was selected as the most suitable variant of processing. A total of 4 locations were selected for detailed microstructure analysis, i. e., the first location observed was near the surface, followed by the location close to the inflection point at the hardness drop, the region of minimum hardness is the third location and the region of the base material represents the fourth location. These locations are depicted in Fig. 6 by red ellipses.

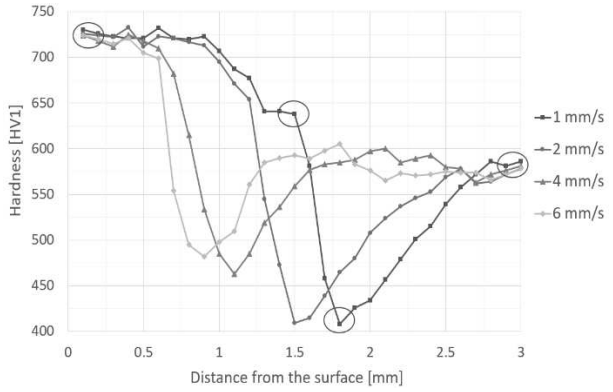

Fig. 6 *Hardness profiles measurement with differing traverse speed and with selected areas for analysis (red ellipses)*

3.3 Metallography

The microstructural features of the steel correlated reasonably with the hardness values (Fig. 6 – blue line). The effect of laser surface hardening of H11 tool steel was observed using light and electron microscopy. The overview image in Fig. 7a captured the laser-hardened surface of H11 tool steel with measured hardness profile indents in a cross-sectional general overview. The microstructure of the laser re-austenitised surface region (0.2 mm below the surface) was characterized by lath martensite with a sparse presence of coarse undissolved carbide particles (Fig. 7b, Fig. 8a). The inter-dendritic carbidic network in the top laser-affected zone reported by Šebek et al. [11], was not observed. The over-tempered zone [12] at a depth of about 1.8 mm (Fig. 7d, Fig. 8c), characterized by the minimum hardness values, exhibited a higher degree of over-tempered martensite compared to the microstructure in the 1.5 mm region (Fig. 7c, Fig. 8b). The carbidic phase in the region 1.8 mm below the surface was composed of fine dispersed particles of various shapes (spherical, elliptical, etc.), which precipitated both along and inside the martensite laths. The microstructure at a depth of 3.0 mm (Fig. 7e, Fig. 8d) was formed by tempered martensite with fine carbides distributed mainly along the martensite laths. If the microstructure of the base material is compared with the microstructure in the surface area, the martensitic laths have been refined by laser remelting, which is in agreement with studies by Šebek and Zhang et al. [11, 13].

In the sub-surface areas 0.2 and 1.5 mm, the measured original (prior) austenite grain size (PAG) reached G 10.0 according to ISO 643 values. In these areas, complete (0.2 mm) or partial (1.5 mm) austenitization took place, due to which a refinement of the PAG was observed compared to the base material (G 8.5) PAG.

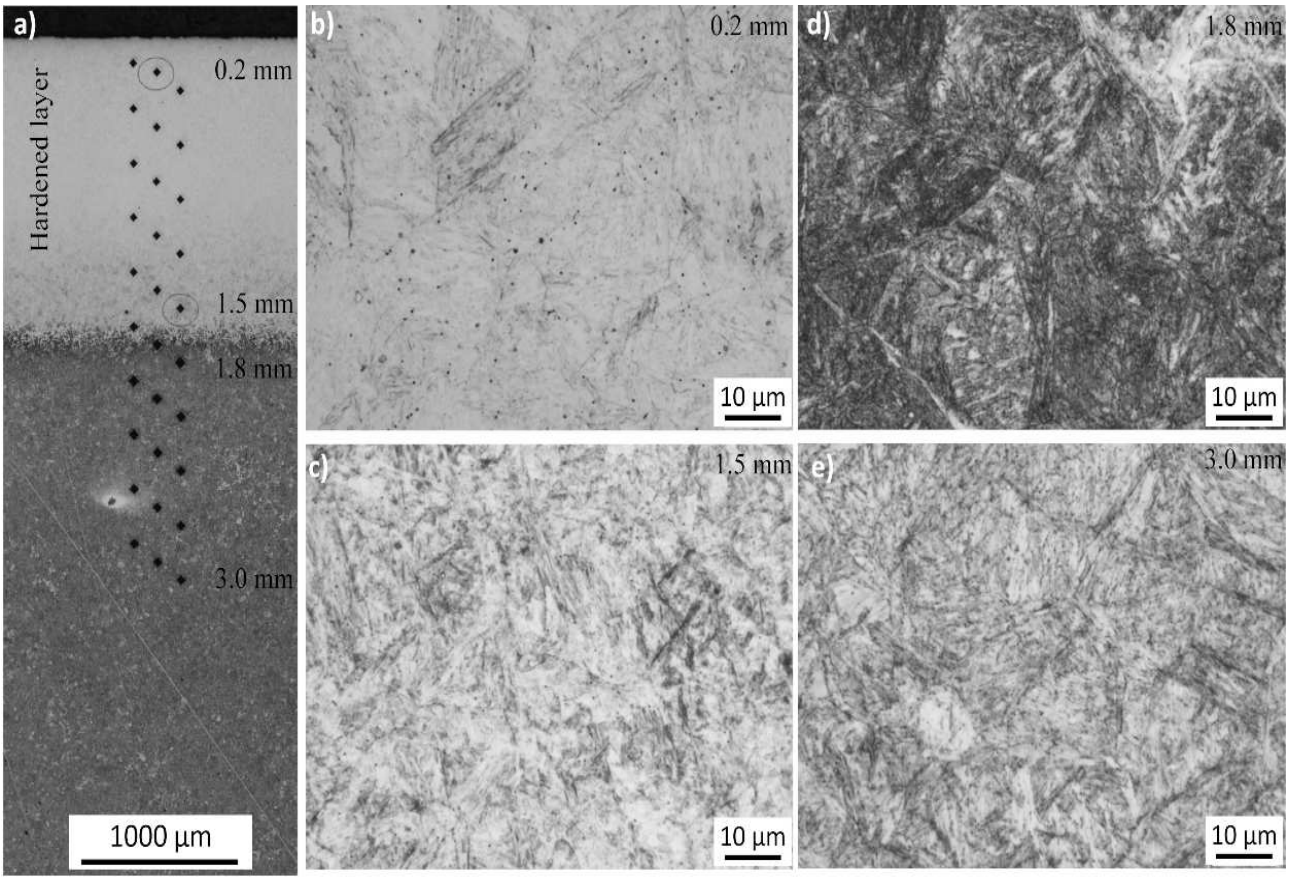

Fig. 7 *Microstructure in the most important positions analysed by light microscopy: a) cross-section microstructure overview; b) 0.2 mm; c) 1.5 mm; d) 1.8 mm; e) 3.0 mm*

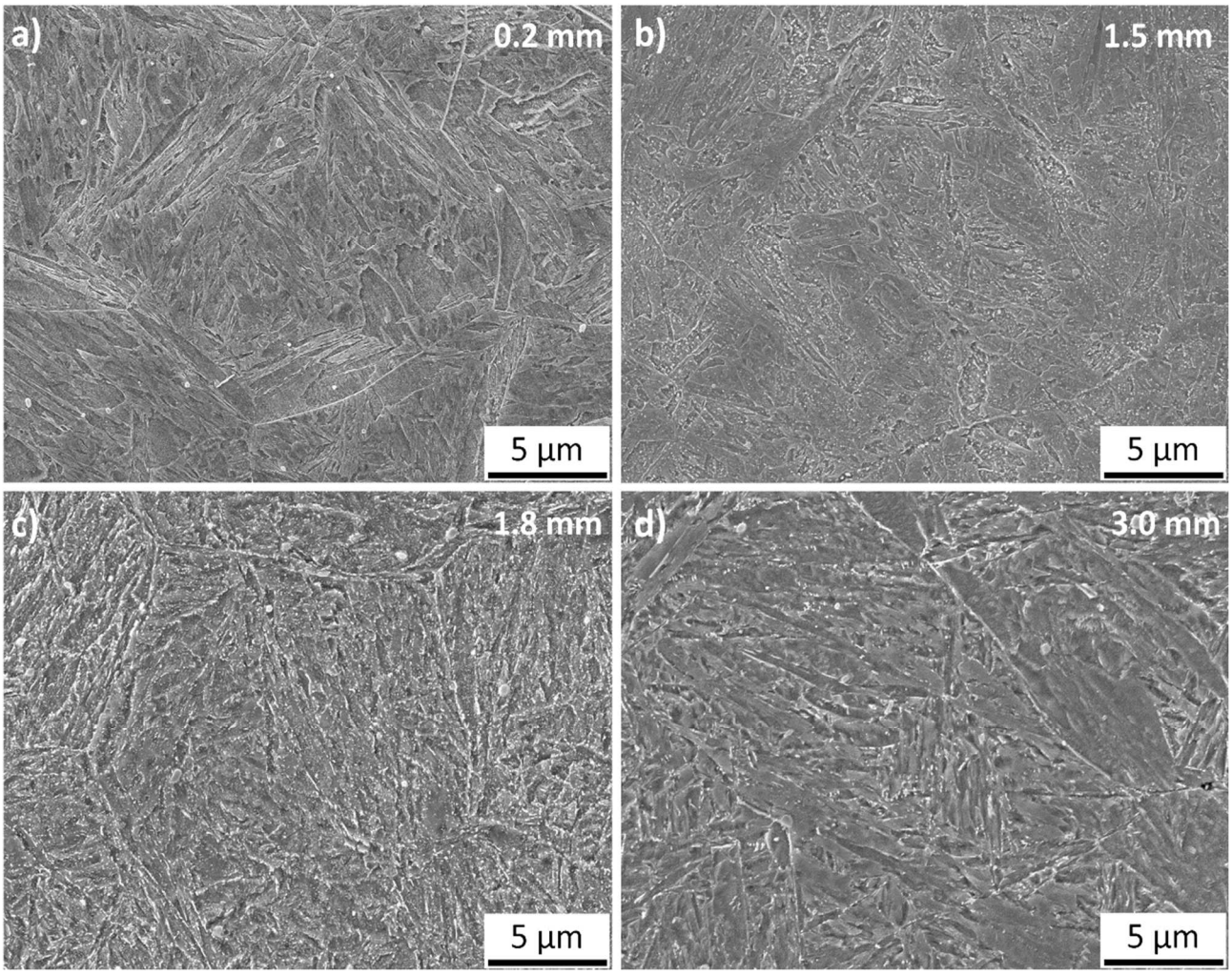

Fig. 8 *Detailed microstructures of analysed localities at: a) 0.2 mm; b) 1.5 mm; c) 1.8 mm; d) 3.0 mm*

The main alloying elements of H11 steel, i.e., Cr, Mo and V, may either act as precipitation strengthening elements by joining with C to form alloy carbides, or may dissolve into the matrix, as a result causing the solution to strengthen the alloy [13]. The energy dispersive spectroscopy (EDS) [14], results analysed at 0.2 mm and 1.8 mm (Fig. 9, Tab. 3) demonstrated the presence of the carbide phase in the matrix, mainly including V-rich MC carbides, Cr-rich M_7C_3 carbides and $M_{23}C_6$ carbides, and Mo-rich M_2C carbides [15, 16]. The presence of carbide particles rich in Mo, V and Cr (Fig. 9a) indicates that they were not dissolved in the matrix during the laser exposure of the H11 surface layer.

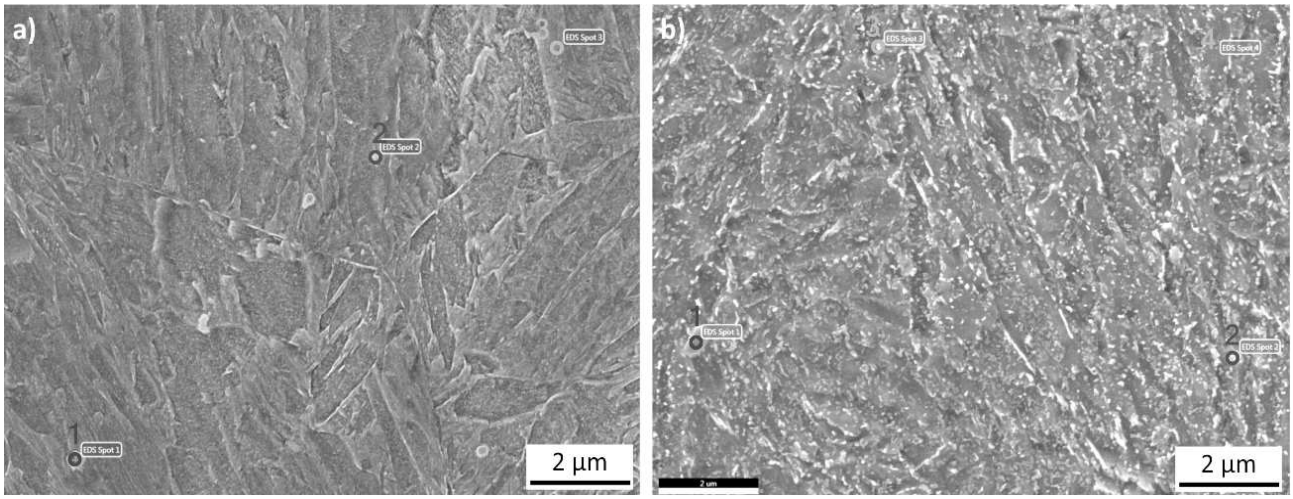

Fig. 9 *Localities of EDS analysis: a) 0.2 mm; b) 1.8 mm*

Tab. 3 *Chemical composition measured at distances 0.2 mm and 1.8 mm from the surface. Weight %.*

Spot	0.2 mm			1.8 mm			
	1	2	3	1	2	3	4
Si	1.3	1.4	1.2	1.2	1.4	1.2	1.1
Mo	1.3	2.7	0.9	4.2	2.8	1.2	0.9
V	3.4	0.8	0.5	18.7	9.7	0.7	0.4
Cr	5.8	5.6	5.7	5.5	6.5	8.2	5.9
Fe	Bal.	Bal.	Bal.	Bal.	Bal.	Bal.	Bal.

4 Discussion

The FEM model was created in DEFORM-3D and the temperature distribution was validated through experimental temperature measurements. The numerical model considered the phase transformation kinetics based on the simplified Avrami equation. The transformation from one phase to another is determined only by the temperatures reached and does not consider time as an additional parameter despite this simplification, the FEM model yields results that are consistent with experimentally observed trends and can be used to estimate temperatures and hardness. The structures were defined as initial structure (SS), intermediate structure (IS), and newly transformed martensite from the austenite during the LSH process especially near the surface area (FS). The expected values of surface hardness, lowest hardness point, and initial as quenched and tempered state were set by the measurement. The obtained results show the expected hardness distribution and the maximum temperature reached depending on the depth after LSH.

Measurements of hardness distribution after the performed experiment by LSH with varying traverse speeds show good agreement with the numerical simulation. The best hardness distribution values were obtained using 1 mm/s traverse speed. The depth after LSH was about 1.6 mm, the surface hardness was up to 730 HV1, and the maximum hardness drop was up to 405 HV1. The trend of the hardness curves after increasing the traverse speed was identical to the numerical simulation results. The depth of the laser-hardened layer decreased with increasing traverse speed and at the same time the hardness drop caused by martensite over-tempering becomes shallower and narrower.

Metallography was investigated in 4 different areas of LSH for the 1 mm/s traverse speed used. The microstructure was analysed at selected depths: 0.2 mm, 1.5 mm, 1.8 mm, and 3.0 mm. All these depths represent a different type of microstructure obtained during the LSH process. The difference between depths 1.5 mm and 1.8 mm consists of a higher amount of over-tempered martensite in the case of the region at depth 1.8 mm. A zone appears near the interface of laser quenched and non-quenched material, where the structure is partially austenitized and partially only high-tempered. In this zone, the proportion of the austenitized structure changes and converges to zero with increasing depth. Below this band is the structure of the over-tempered martensite itself and past it the unaffected core of the tool. The carbidic phase in the region 1.8 mm below the surface was composed of very fine dispersed particles of various shapes, which precipitated both along and inside the martensite laths. The core of steel in-depth 3.0 mm was formed by tempered martensite with fine carbides distributed mainly along the martensite laths, coarser compared to surface martensite with very fine laths. EDS analysis is done at depths 0.2 mm and 1.8 mm and shows the presence of the carbide phase in the matrix, mainly including V-rich MC carbides, Cr-rich M_7C_3 carbides, and $M_{23}C_6$ carbides and Mo-rich M_2C carbides at both analysed depths. A moderate effect of full/partial austenitization in the sub-surface localities on PAG size was observed.

5 Conclusion

The aim of this research was to evaluate the effect of different laser traverse speeds in the laser surface hardening process. A numerical simulation of the LSH was performed to analyse behavior and trends of hardness curves and expected laser hardening depth. The calculation of the temperature displacement shows a correlation with the hardness curves. The maximum drop in hardness was recorded at approx. 750 °C in the HAZ. Experimental verification of the results was performed using the selected parameters. The resulting curves of hardness distribution show the same trend compared with a numerical model. The most promising results were obtained using a traverse speed of 1 mm/s, the maximum increased depth was about 1.6 mm, with surface hardness up to 730 HV1. The minimum hardness measured at a depth of about 1.8 mm was 405 HV1 in the over-tempered zone. The LSH of the H11 tool steel led to complex microstructural changes caused by the temperature gradient. Four zones, identified by significant changes in hardness value, were analysed by means of light and scanning electron microscopy. The presence of carbide particles rich in Mo, V, and Cr was confirmed by EDS analysis. In the surface area, the martensitic laths were refined by surface hardening.

Acknowledgement

The result was supported from ERDF Research of advanced steels with unique properties, No. CZ02.1.01/0.0/0.0/16_019/0000836.

References

[1] UMEMOTO, M., HAI GUO, Z., TAMURA, I. (2013). Effect of cooling rate on grain size of ferrite in a carbon steel. In. *Mater Science and Technology*, Vol. 3, No. 4, pp. 249-255, ISSN 0267-0836

[2] DAS, A., SUNIL, S., KAPOOR, R. (2019). Effect of Cooling Rate on the Microstructure of a Pressure Vessel Steel. In. *Metallography, Microstructure, and Analysis,* Vol. 8, No. 6, pp. 795-805, ISSN 2192-9262

[3] ALI, M., PORTER, D., KÖMI, J., EISSA, M., EL FARAMAWY, H., MATTAR, T. (2019). Effect of cooling rate and composition on microstructure and mechanical properties of ultrahigh-strength steels. In. *Journal of Iron and Steel Research International.* Vol. 26, No. 12, pp. 1350-1365, ISSN 0267-0836

[4] ŠRAMHAUSER, K., KUŚMIERCZAK, S. (2016). Laser Hardening of Functional Surface of Machine Tools. In. *Manufacturing Technology.* Vol 16, No. 1, pp. 248-253, ISSN 1213-2489

[5] DAUSINGER, F., SHEN, J. (1993). Energy Coupling Efficiency in Laser Surface Treatment. In. *ISIJ International.* Vol. 33, No. 9, pp. 925-933, ISSN 0915-1559

[6] MUTHUKUMARAN, G., DINESH BABU, P. (2021). Laser transformation hardening of various steel grades using different laser types. In. *Journal of the Brazilian Society of Mechanical Sciences and Engineering.* Vol. 43, No. 2, ISSN 1678-5878

[7] JERNITI, A.G., El OUAFI, A., BARKA, N. (2016). A Predictive Modeling Based on Regression and Artificial Neural Network Analysis of Laser Transformation Hardening for Cylindrical Steel Workpieces. In. *Journal of Surface Engineered Materials and Advanced Technology*. Vol. 6, No. 4, pp. 149-163. ISSN 2161-4881

[8] ABORKIN, A. V., VAGANOV, V. E., SHLEGEL', A. N., BUKAREV, I. M. (2015). Effect of Laser Hardening on Die Steel Microhardness and Surface Quality. In. *Metallurgist.* Vol. 59, No 7-8, pp. 619-625, ISSN 0026-0894

[9] GIORLEO, L., PREVITALI, B., SEMERARO, Q. (2011). Modelling of back tempering in laser hardening. In. *The International Journal of Advanced Manufacturing Technology*. Vol. 54, No. 9-12, pp. 969-977, ISSN 0268-3768

[10] LEE, J. H., JANG, J. H., JOO, B. D., SON, Y. M., MOON, Y. H. (2009). Laser surface hardening of AISI H13 tool steel. In. *Transactions of Nonferrous Metals Society of China.* Vol. 19, No. 4, pp. 917-920, ISSN 1003-6326

[11] ŠEBEK, M., FALAT, L., KOVÁČ, F., PETRYSHYNETS, I., HORŇAK, P., GIRMAN, V. (2017). The Effects of Laser Surface Hardening on Microstructural Characteristics and Wear Resistance of AISI H11 Hot Work Tool Steel. In. *Archives of Metallurgy and Materials*. Vol. 62, No. 3, pp. 1721-1726, ISSN 2300-1909

[12] TELASANG, G., DUTTA MAJUMDAR, J., PADMANABHAM, G., MANNA, I. (2014). Structure–property correlation in laser surface treated AISI H13 tool steel for improved mechanical properties. In. *Materials Science and Engineering: A.* Vol. 599, pp. 255-267, ISSN 0921-5093

[13] ZHANG, J., YU. M., LI. Z., LIU, Y., ZHANG, Q., JIANG, R., SUN. S. (2021). The effect of laser energy density on the microstructure, residual stress and phase composition of H13 steel treated by laser surface melting. In. *Journal of Alloys and Compounds*, Vol. 856, ISSN 0925-8388

[14] KOVÁČIKOVÁ, P., DUBEC, A., KOŠTIALIKOVÁ, D., JANEKOVÁ, M. (2020). Examination of surface wear on the timing chain tensioner depending on the engine oil contamination. In. *Manufacturing Technology*. Vol. 20, No. 4. Pp 463-467, ISSN 1213-2489

[15] MARTÍNEK, P., PODANÝ, P., NACHÁZEL, J. (2015). Decreasing the carbonitride size and amount in austenitic steel with heat treatment and thermomechanical processing, In. *Materiali in Tehnologije*, Vol. 49, No. 1, pp. 31-36, ISSN 1580-2949

[16] MARTÍNEK, P., PODANÝ, P. (2020). Image analysis of titanium carbonitrides. In: *Proceedings 29th International Conference on Metallurgy and Materials*, pp. 527-532, ISSN 2694-9296